ChemPubSoc Europe

DOI: 10.1002/cmdc.201500552

CHEMMEDCHEM Full Papers

Reactivity, Selectivity, and Reaction Mechanisms of Aminoguanidine, Hydralazine, Pyridoxamine, and Carnosine as Sequestering Agents of Reactive Carbonyl Species: A Comparative Study

Mara Colzani,* Danilo De Maddis, Gaia Casali, Marina Carini, Giulio Vistoli, and Giancarlo Aldini[a]

Reactive carbonyl species (RCS) are endogenous or exogenous byproducts involved in the pathogenic mechanisms of different oxidative-based disorders. Detoxification of RCS by carbonyl quenchers is a promising therapeutic strategy. Among the most studied quenchers are aminoguanidine, hydralazine, pyridoxamine, and carnosine; their quenching activity towards four RCS (4-hydroxy-*trans*-2-nonenal, methylglyoxal, glyoxal, and malondialdehyde) was herein analyzed and compared. Their ability to prevent protein carbonylation was evaluated in vitro by using an innovative method based on high-resolution mass spectrometry (HRMS). The reactivity of the compounds was RCS dependent: carnosine efficiently quenched 4-hydroxy-*trans*-2-nonenal, pyridoxamine was particularly active towards malondialdehyde, aminoguanidine was active towards methylglyoxal and glyoxal, and hydralazine efficiently quenched all RCS. Reaction products were generated in vitro and were characterized by HRMS. Molecular modeling studies revealed that the reactivity was controlled by specific stereoelectronic parameters that could be used for the rational design of improved carbonyl quenchers.

Introduction

Reactive carbonyl species (RCS) are a class of byproducts arising from exogenous and endogenous oxidation. RCS can covalently react with nucleophilic targets such as proteins, phospholipids, and nucleic acids to form damaging adducts.[1] According to their structure, RCS are generally grouped into three main chemical classes: 1) α,β-unsaturated aldehydes, for example, 4-hydroxy-*trans*-2-nonenal and acrolein; 2) keto aldehydes, for example, methylglyoxal; 3) dialdehydes, for example, glyoxal and malondialdehyde.[2] Proteins represent the most studied target of RCS; the corresponding reaction products are named advanced lipoxidation end products (ALEs) or advanced glycation end products (AGEs), depending on the origin of the attacking RCS (lipids or sugars, respectively).

For several decades, RCS and their reaction products have been considered as markers of oxidative stress,[3] and this was based on the observation of a correlation between disease states and the amount of RCS and AGEs/ALEs in tissue and fluid, in both animals and humans. Several analytical attempts to measure them in biological matrices have been reported. In addition, the implication of RCS in different physiopathological conditions has been reported, highlighting their toxic role.[4] The involvement of RCS in the onset and progression of human diseases is supported by the following facts: 1) a substantial amount of literature reporting the molecular and cellular pathogenic mechanisms for RCS involvement in the onset and progression of different diseases, including atherosclerosis,[5] diabetes,[6] and some neurological disorders is now available;[7] 2) compounds effective as inhibitors of AGEs/ALEs and/or as detoxifying agents of RCS or those that are able to block their biological effects significantly counteract different oxidative stress based diseases.[8]

Hence RCS, besides being considered biomarkers of oxidative stress, also represent promising drug targets, and molecular approaches targeting their toxic effects have led to promising results.[1,9] Among the molecular approaches aimed at inhibiting protein modification by RCS (protein carbonylation), scavenging of RCS is a promising one.[10] It is based on small nucleophilic molecules (RCS-sequestering agents or carbonyl quenchers) able to covalently react with RCS to form unreactive and hydrophilic reaction products. The reactive group present on the RCS-sequestering agents can be of different types; for instance, thiol-containing sequestering agents (such as D-penicillamine[11]) as well as guanidine[12] and hydrazine[13] derivatives have been reported to prevent the formation of ALEs and AGEs by reacting with different types of RCS.

L-Carnosine (CAR), hydralazine (HY), pyridoxamine (PM), and aminoguanidine (AG) are among the most-studied RCS-sequestering agents, so far. These compounds have been reported to react with RCS belonging to the different classes and have also been reported to be effective in several animal models, for

[a] Dr. M. Colzani, Dr. D. De Maddis, G. Casali, Prof. M. Carini, Prof. G. Vistoli, Prof. G. Aldini
Department of Pharmaceutical Sciences, Università degli Studi di Milano
via Mangiagalli, 25, 20133 Milano (Italy)
E-mail: mara.colzani@unimi.it

Supporting Information and the ORCID identification number(s) for the author(s) of this article can be found under http://dx.doi.org/10.1002/cmdc.201500552.

which RCS are considered to act in the onset and progression of diseases.[1,14] Moreover, the direct RCS-sequestering effect has been demonstrated under in vivo conditions by identifying the corresponding reaction products in urine and serum.[15] The chemical structures of the RCS-sequestering agents mentioned above are quite heterogeneous: HY and AG are monoreactive carbonyl quenchers presenting a reactive hydrazine group, whereas CAR and PM are polyreactive carbonyl quenchers. In particular, CAR is a dipeptide bearing an amino group and an imidazole ring, whereas PM is a phenyl derivative presenting a primary amino group and a phenolic function involved in the quenching mechanisms.[16] Such chemical diversity suggests that the reactivity of these sequestering agents towards the different classes of RCS should be different.

Although several studies have reported the reactivity of sequestering agents towards given RCS, no comparative studies on their reactivity towards the most abundant RCS is available; furthermore, neither a systematic study of the reaction mechanism nor comprehensive elucidation of the reaction products has been reported. In the present paper, the ability of L-carnosine, hydralazine, pyridoxamine, and aminoguanidine to dose-dependently inhibit the protein carbonylation of ubiquitin induced by four different RCS—4-hydroxynonenal (HNE), methylglyoxal (MGO), glyoxal (GO), and malondialdehyde (MDA)—is compared and rationalized in terms of density functional theory (DFT)-based quantum-mechanical descriptors. The rationale of using ubiquitin as a model protein was recently described;[17,18] notably, the lack of cysteine residues in the sequence of this protein allows the observation of a variety of RCS-derived modifications on different nucleophilic residues (i.e., lysine, arginine, and histidine), which would otherwise be masked or flattened by the high reactivity of cysteine.[19] Moreover a comprehensive study on the reaction products generated in vitro by the incubation of RCS and sequestering agents (as detected by high-resolution mass spectrometry, HRMS) is also provided, together with the reaction mechanisms leading to their formation.

Results

Sequestering activity and selectivity

Direct sequestering activity

As a first strategy to measure the quenching activities towards HNE and MGO, these RCS were incubated with the sequestering agents L-carnosine, pyridoxamine, hydralazine, and aminoguanidine. Adduct formation was indirectly assessed by measuring the consumption of RCS by HPLC–UV. To mimic physiological conditions, the assays were performed by using a saline buffer at pH 7.4.

Table 1 collects the sequestering activities measured for HNE, MGO, and pyridoxal, as detected by HPLC. They were obtained by monitoring the consumption percentages (Q%) of the carbonyl species after 24 h, considering several quencher/RCS ratios ranging from 1:10 to 10:1. Table 1 reports $Q\%_{1:1}$ values (computed at a RCS/quencher ratio of 1:1), together with the R_{50} values expressing the molar ratio between sequestering agent and RCS producing 50% of carbonyl consumption. According to the R_{50} values, the activity ranking toward HNE is HY > CAR > AG > PM, whereas that for MGO is HY > AG > CAR > PM. In both cases, HY is the most efficient sequestering agent and PM is the least effective one. The direct sequestering activity towards GO and MDA was not assayed because these carbonyl species were not detectable by our experimental setup.

Table 1. Direct quenching activities as determined by HPLC–UV analysis of the reactive carbonyl species (RCS)-sequestering agents, aminoguanidine (AG), hydralazine (HY), pyridoxamine (PM), and L-carnosine (CAR), tested towards 4-hydroxynonenal (HNE), methylglyoxal (MGO), and pyridoxal.

	HNE		MGO		pyridoxal
	$Q\%_{1:1}$[a]	R_{50}[b]	$Q\%_{1:1}$[a]	R_{50}[b]	$Q\%_{10:1}$[a]
CAR	37.28 ± 2.29	1.52	12.82 ± 1.62	3.96	0.01 ± 0.98
PM	2.11 ± 0.47	11.78	2.47 ± 1.38	9.31	2.15 ± 0.08
HY	87.21 ± 3.16	0.33	48.65 ± 4.19	0.85	100.0
AG	2.27 ± 0.69	8.40	34.72 ± 2.67	1.67	12.79 ± 0.09

[a] Q% values express the percentages of RCS reacted in the presence of the tested quenchers after 24 h incubation by using a molar ratio of quencher/aldehyde equal to 1:1 ($Q_{1:1}$%) or 10:1 ($Q_{10:1}$%). The standard error values refer to two independent replicates. [b] R_{50} values express the quencher/RCS molar ratio yielding 50% adduct formation, as referred to the initial concentration of reactants.

In addition to HNE and MGO, the activity towards pyridoxal was also measured to establish the selectivity of the different sequestering agents for this endogenous aldehyde. Given that this quenching is an undesired feature, Table 1 shows the consumption percentages as obtained for the most challenging 10:1 ratio ($Q\%_{10:1}$ instead of $Q\%_{1:1}$ data). The $Q\%_{1:10}$ values show limited quenching activity of CAR and PM towards pyridoxal, whereas AG exhibits moderate activity ($Q\%_{10:1}$ = 12.79%). HY shows remarkable quenching activity towards pyridoxal ($Q\%_{10:1}$ = 100%); these data are in good agreement with the well-known lack of selectivity of HY[20] and AG.[21] Overall, these data indicate satisfactory selectivity of CAR and PM for HNE and MGO.

Inhibition of carbonylation

To further investigate the quenching ability of different sequestering agents toward RCS, a protein-based competitive assay was developed. In this approach, RCS were incubated in vitro with a target protein (ubiquitin) in the presence of different concentrations of carbonyl quenchers; after incubation, the extent of protein carbonylation was measured by HRMS. Figure 1a shows the mass spectrum of control ubiquitin (incubated at 10 μM concentration without RCS and quenchers); the spectrum acquired under denaturing, acidic conditions is characterized by a typical pattern of multicharged ions ranging from +7 to +13; the +11 peak at m/z = 779.61064 is the most intense signal (Figure 1b). The deconvoluted mass spectrum shows that the experimental mass value is in agreement with the expected average mass of ubiquitin (8564.74 Da).

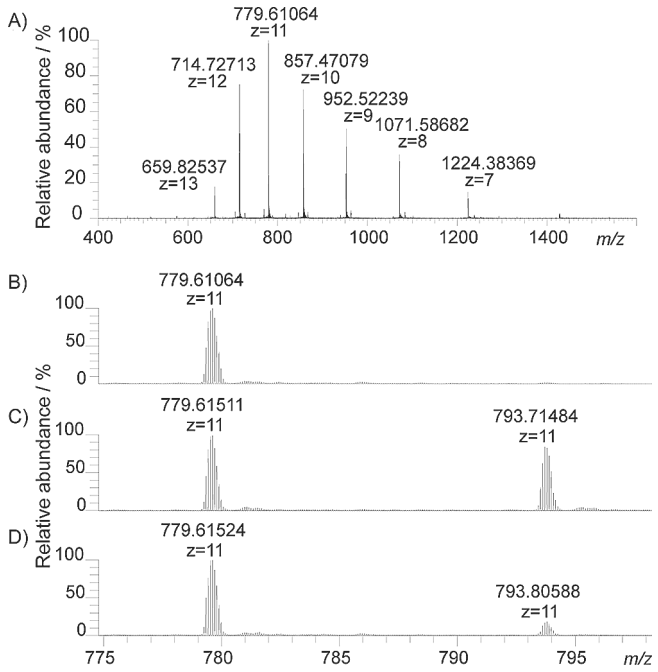

Figure 1. Rationale of the carbonyl quenching assay based on ubiquitin and high-resolution MS. a) Multicharged ions pattern of unmodified ubiquitin upon in vitro incubation with neither RCS nor sequestering agent (control sample); b) focus on the 11+ peak of the control sample ($m/z = 779$); c) 11+ peaks obtained upon incubating ubiquitin with HNE, corresponding to unmodified ($m/z = 779$) and HNE-modified ($m/z = 793$) forms of the protein; d) 11+ peaks obtained upon incubating ubiquitin with HNE and carnosine, showing reduced intensity for the peak corresponding to the modified protein ($m/z = 793$). Figure legend: *z*, charge.

As we recently reported,[18] additional multicharged ions appear if ubiquitin is incubated in vitro with the reactive carbonyl species 4-hydroxynonenal, methylglyoxal, glyoxal, or malondialdehyde, and this was attributed to the corresponding covalent adducts. In pursuit of clarity, we chose to focus on the +11 peaks as representatives of the different peaks visible in the mass spectra.

As an example, Figure 1c shows the +11 peaks in the mass spectra relative to 10 μM ubiquitin incubated with 500 μM HNE (50-fold molar excess). The +11 peak at $m/z = 779$ (corresponding to unmodified ubiquitin still present in the sample) is flanked by an additional peak at a higher mass-to-charge ratio ($m/z = 793$), which corresponds to modified ubiquitin that underwent covalent Michael adduction by HNE.[18]

Ubiquitin was co-incubated with 1) each of the RCS, that is, HNE, MGO, GO, and MDA, at a fixed concentration able to generate approximately 50% of carbonylated ubiquitin; 2) increasing concentrations of each of the sequestering agents, that is, CAR, PM, HY, and AG.

As an example, Figure 1d shows the +11 peaks obtained upon co-incubation of 10 μM ubiquitin with 500 μM HNE and 1 mM L-carnosine (2× molar excess of quencher vs. HNE): the inhibition of protein carbonylation is visible as a reduction in the intensity of the peak corresponding to modified ubiquitin ($m/z = 793$) relative to the intensity of unmodified ubiquitin ($m/z = 779$). Figures S1–S4 (Supporting Information) show the +11 peaks obtained by HRMS upon incubation of ubiquitin with HNE, MGO, GO, and MDA in the presence of increasing concentrations of the quenchers. All sequestering agents totally or partially inhibited the formation of the carbonylated forms of ubiquitin in a dose-dependent manner.

Quantification of the sequestering activity

The ability of each sequestering agent to inhibit ubiquitin carbonylation was determined by measuring the percentage of modified ubiquitin, as explained in the Experimental Section. The percentage of modified ubiquitin detected at increasing concentrations of each quencher was used to obtain dose–response curves (Figure 2). The carbonyl sequestering activity was expressed by calculating the molar excess of each sequestering agent able to reduce the formation of ubiquitin adducts by 50% (UC_{50}). UC_{50} values are expressed with respect to the concentration of RCS present in each sample, with a view to compare the reactivity of each sequestering agent towards different RCS. The computed UC_{50} values are reported in Table 2. As expected, the tested compounds inhibited the formation of protein adducts with different efficacies. PM efficiently inhibited the formation of GO and MDA adducts, whereas AG and HY showed higher efficacy for MGO- and GO-derived adducts. Conversely, CAR was selective for HNE- and MDA-derived adducts, whereas it inhibited the formation of the GO- and MGO-derived adducts only at elevated concentrations.

Table 2. Quantification of the sequestering activity of aminoguanidine (AG), hydralazine (HY), pyridoxamine (PM), and L-carnosine (CAR) measured by protein carbonylation assay.

	4-hydroxynonenal (HNE)			methylglyoxal (MGO)			glyoxal (GO)			malondialdehyde (MDA)		
	UC_{50}[a]	Std. error[b]	CV[c] [%]	UC_{50}[a]	Std. error[b]	CV[c] [%]	UC_{50}[a]	Std. error[b]	CV[c] [%]	UC_{50}[a]	Std. error[b]	CV[c] [%]
AG	8.97	1.01	11.2	0.50	0.07	13.0	0.55	0.04	8.0	9.41	0.75	7.9
HY	1.21	0.14	11.2	1.19	0.23	18.9	0.51	0.13	25.3	3.11	0.52	16.8
PM	8.82	0.20	14.7	9.29	0.60	6.5	3.27	0.43	0.13	1.31	0.07	5.5
CAR	1.34	0.17	2.0	>100	ND[d]	ND[d]	>50	ND[d]	ND[d]	4.05	0.46	11.4

[a] UC_{50} values obtained from the protein carbonylation assay, expressing the molar excess of each quencher (over RCS concentration) able to reduce the formation of ubiquitin adducts by 50%. [b] Standard error values refer to three independent replicates. [c] CV: coefficient of variation. [d] ND: not determined.

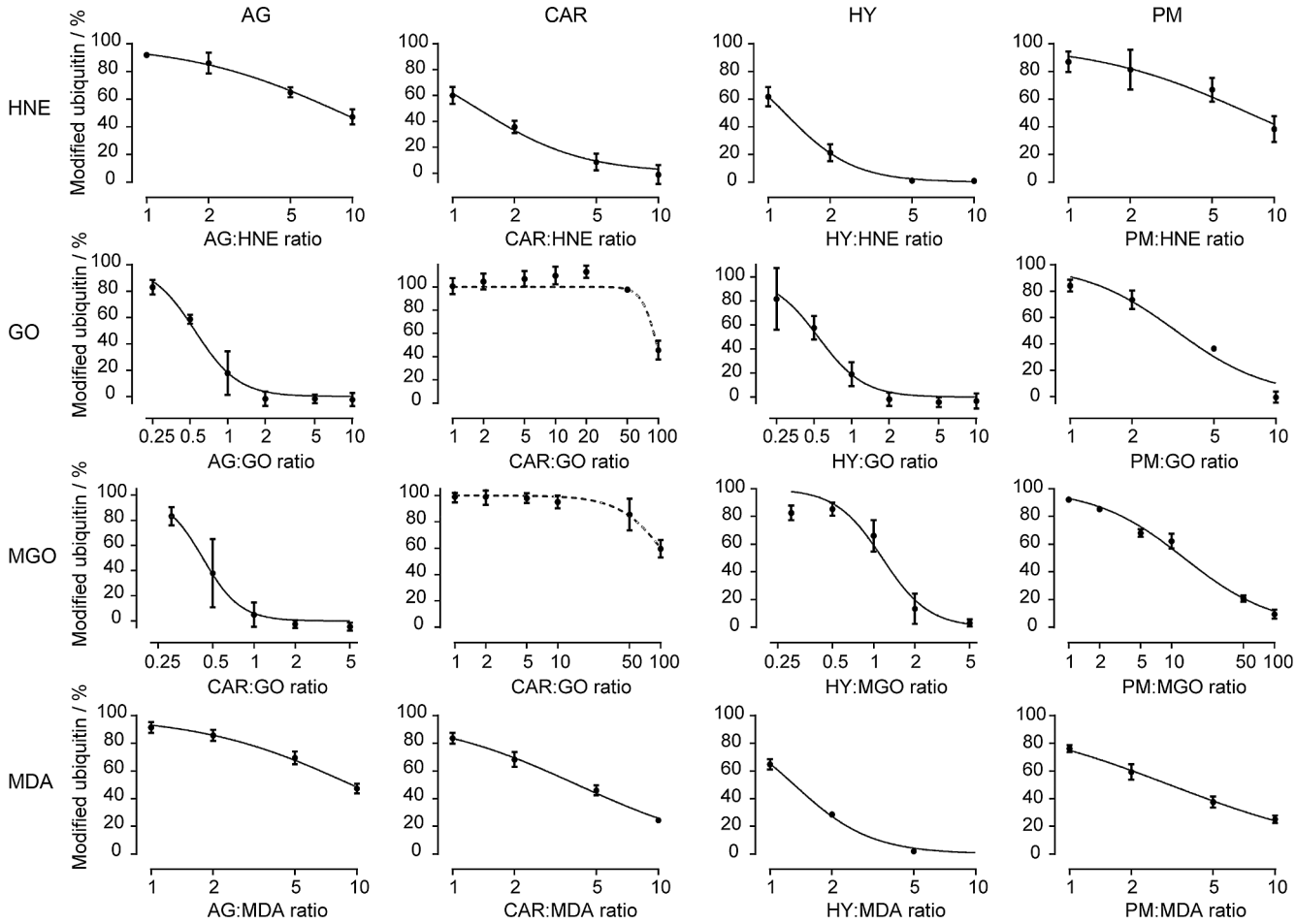

Figure 2. Dose–response curves for quenching experiments performed by co-incubating ubiquitin with the sequestering agents aminoguanidine, carnosine, hydralazine, and pyridoxamine and the reactive carbonyl species HNE, MGO, GO, and MDA. The molar ratio of sequestering agents towards RCS is expressed on a log scale. Curve fitting by nonlinear regression was used to estimate UC_{50} values, corresponding to the molar ratio of sequestering agents over RCS concentration able to prevent the formation of ubiquitin adducts by 50%. Standard errors refer to three independent replicates.

Comparison of the R_{50} and UC_{50} values

The UC_{50} values obtained in the protein carbonylation assay performed with HNE show that HY was the most effective quencher of HNE, followed by CAR, whereas AG and PYR showed less relevant quenching activities. This order of reactivity is similar to that observed in the direct quenching assay, which suggests that the inhibition of protein carbonylation by HNE is mainly regulated by a direct quenching effect. Regarding MGO, the order of reactivity observed in the protein carbonylation assay was AG > HY > PM > CAR, unlike the data obtained in the direct assay. However, in both cases, AG and HY were the most effective quenchers, whereas PM was confirmed to be less effective. In the carbonylation assay, CAR showed a negligible quenching activity, different from the direct assay.

Table S1 reports the correlation matrix between the sequestering activities, measured either as R_{50} in the direct assay or as UC_{50} in the protein carbonylation assay. The table reveals a notable correlation between the R_{50} and UC_{50} values measured for HNE ($r^2 = 0.99$), whereas no correlation is observed for MGO ($r^2 = 0.04$). This suggests that the sequestering activity toward HNE measured in the direct assay at physiological pH is not biased by the formation of reversible/side products. In contrast, the activity towards MGO in the direct assay is either affected by reversible condensation or involves very complex and kinetically disfavored reaction mechanisms, and in both cases, their occurrence in the protein carbonylation assay can be limited. Possible explanations for this phenomenon were investigated by analyzing the reaction products generated by each RCS with each sequestering agent.

Analysis of reaction products by HRMS

The reaction products generated by separately incubating each sequestering agent with HNE, GO, MGO, and MDA were analyzed by HRMS by collecting high-resolution mass spectra and fragmentation spectra. Both types of spectra were used to identify and elucidate the structures of the reaction products. To this end, we applied the following strategy: 1) the experimental, highly accurate mass values obtained by HRMS analysis were used to obtain the elemental composition of the adducts (tolerance = 8 ppm); 2) tentative chemical structures of the adducts were drawn on the basis of the elemental composition and of previously reported structures; 3) the tentative

structures were fragmented in silico; 4) finally the masses of the theoretical fragments were compared with the experimental data to confirm the identity of the precursor ion. Table 3 summarizes the reaction products identified by HRMS. The full mass and fragmentation spectra together with the associated molecular structures are reported in Figures S5–S20. The reactions leading to the formation of the different adducts are proposed in Schemes 1–4.

Reaction products generated by AG

As seen for all the tested sequestering agents, the hydrazine function of AG reacted with the β carbon atom of HNE, which led to the formation of corresponding Michael adduct **1.1**, (*m/z* = 231.18103, Scheme 1). Moreover, the AG hydrazine group condensed with the HNE carbonyl group to yield guanyl hydrazone adduct **1.2** (*m/z* = 213.17058) as previously suggested by Neely on the basis of NMR spectroscopy studies.[22] Upon incubation with GO and MGO, AG generated triazine adducts, a finding that came as no surprise, as the reaction between AG and variously substituted α-dicarbonyls is a well-known method to synthesize 1,2,4-triazine derivatives. Notably, this reaction gives optimized yields under basic conditions but can also occur at physiological pH, as confirmed herein.

With both GO and MGO, the condensation mechanism occurred through the formation of the corresponding guanyl hydrazone intermediate, which then cyclized to generate the final triazine rings. In detail, the condensation between AG and GO first generated 3-amino-6-hydroxy-5,6-dihydro-1,2,4-triazine (**1.3**, *m/z* = 115.06055), and this species finally dehydrated to yield 3-amino-1,2,4-triazine (**1.4**, *m/z* = 97.05012). Even though the asymmetric structure of MGO can yield two different guanyl hydrazone intermediates, its observed condensation with MGO was highly regioselective, as the obtained fragmentation pattern was compatible only with 3-amino-5-methyl-6-hydroxy-5,6-dihydro-1,2,4-triazine (**1.5**, *m/z* = 129.07648), which dehydrated to give final triazine adduct **1.6** (i.e., 3-amino-5-methyl-1,2,4-triazine; *m/z* = 111.06606); isomeric 3-amino-6-methyl-1,2,4-triazine was not detected. Whereas triazine adduct **1.6** has already been described,[23,24] an unreported ditriazine adduct was also identified that plausibly came from dimerization of **1.6** [i.e., 5-methyl-N^6-(5-methyl-1,2,4-triazin-3-yl)-5,6-dihydro-1,2,4-triazine-3,6-diamine, **1.7**; *m/z* = 221.12509]. In contrast, Saraiva et al. described the formation of bicyclic dihy-

Table 3. Reaction products obtained by the in vitro reaction of the sequestering agents aminoguanidine (AG), pyridoxamine (PM), hydralazine (HY), and L-carnosine (CAR) with the tested reactive carbonyl species (RCS), 4-hydroxynonenal (HNE), glyoxal (GO), methylglyoxal (MGO), and malondialdehyde (MDA).

RCS	Structure	Reaction product	Experimental *m/z*[a]	Theoretical *m/z*	Error [ppm]	Formula	Ref.	Figure
Quencher = AG								
HNE	**1.1**	Michael adduct	231.18103	231.18156	2.3	$C_{10}H_{22}N_4O_2$		S5
HNE	**1.2**	guanyl hydrazone	213.17058	213.17099	1.9	$C_{10}H_{20}N_4O$	[22]	S5
GO	**1.3**	3-amino-6-hydroxy-5,6-dihydro-1,2,4-triazine	115.06055	115.06144	7.7	$C_3H_6N_4O$		S9
GO	**1.4**	3-amino-1,2,4-triazine	97.05012	97.05088	7.8	$C_3H_4N_4$		S9
MGO	**1.5**	3-amino-5-methyl-6-hydroxy-5,6-dihydro-1,2,4-triazine	129.07648	129.07709	4.7	$C_4H_8N_4O$		S13
MGO	**1.6**	3-amino-5-methyl-1,2,4-triazine	111.06606	111.06653	4.2	$C_4H_6N_4$	[23]	S13
MGO	**1.7**	ditriazine	221.12509	221.12577	3.1	$C_8H_{12}N_8$		S13
MDA	**1.8**	5-hydroxy-2*H*-pyrazoline-1-carboxamidine	ND	129.07709	–	$C_4H_8N_4O$	[25]	S17
MDA	**1.9**	1*H*-pyrazole-1-carboxamidine	ND	111.06653	–	$C_4H_6N_4$	[25]	S17
Quencher = PM								
HNE	**2.1**	Michael adduct	325.21223	325.21219	−0.1	$C_{17}H_{28}N_2O_4$		S6
GO	**2.2**	piperazine-based five-ring adduct	417.17478	417.17687	5.0	$C_{20}H_{24}N_4O_6$	[26]	S10
MGO	**2.3**	MOLD-like structure	385.18637	385.18703	1.7	$C_{20}H_{25}N_4O_4$	[27]	S14
MDA	**2.4**	*N*-propenal–pyridoxamine	223.10748	223.10772	1.1	$C_{11}H_{14}N_2O_3$		S18
Quencher = HY								
HNE	**3.1**	Michael adduct	317.19695	317.19721	0.8	$C_{17}H_{24}N_4O_2$		S7
HNE	**3.2**	phthalazinyl hydrazone	299.18639	299.18664	0.8	$C_{17}H_{22}N_4O$		S7
GO	**3.3**	phthalazinyl hydrazone	201.07598	201.07709	5.5	$C_{10}H_8N_4O$		S11
GO	**3.5**	dihydrazone	343.14026	343.14142	3.4	$C_{18}H_{14}N_8$		S11
MGO	**3.4**	phthalazinyl hydrazone	215.09236	215.09274	1.8	$C_{11}H_{10}N_4O$		S15
MGO	**3.6**	dihydrazone	357.15638	357.15707	1.9	$C_{19}H_{16}N_8$		S15
MDA	**3.7**	*N*-propenal–hydralazine	215.09249	215.09274	1.2	$C_{11}H_{10}N_4O$		S19
Quencher = CAR								
HNE	**4.1**	Schiff base	365.21820	365.21834	0.4	$C_{18}H_{28}N_4O_4$	[29]	S8
HNE	**4.2**	Michael adduct	383.22854	383.22890	0.9	$C_{18}H_{30}N_4O_5$	[29]	S8
GO	**4.3**	GOLD-like structure	487.20212	487.20481	5.5	$C_{21}H_{27}N_8O_6$		S12
GO	**4.5**	piperazine-based tricyclic adduct	533.20701	533.21029	6.2	$C_{22}H_{28}N_8O_8$		S12
MGO	**4.4**	MOLD-like structure	501.21974	501.22046	1.4	$C_{22}H_{29}N_8O_6$		S16
MDA	**4.6**	*N*-propenal–carnosine	281.12372	281.12444	2.6	$C_{12}H_{16}N_4O_4$		S20

[a] Experimental *m/z* refers to the values observed in the mass spectra (Figures S5–S20, reporting both MS and MS^n spectra). ND: not determined.

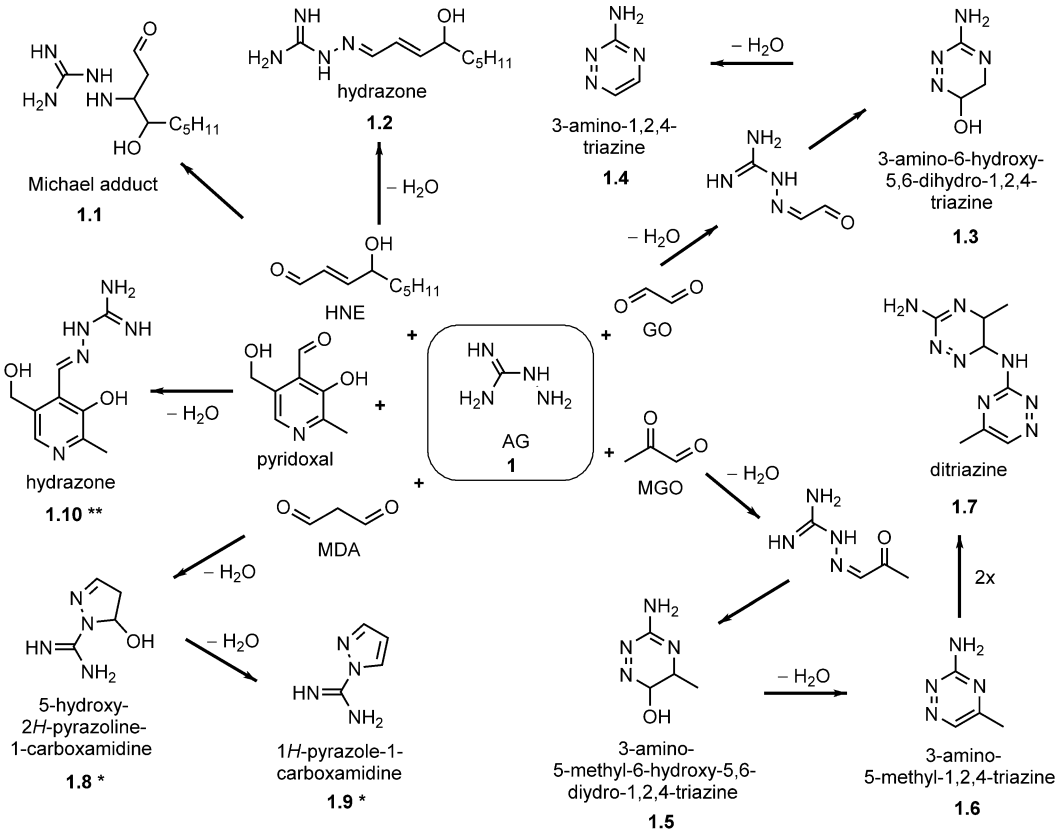

Scheme 1. Reaction products formed by aminoguanidine and HNE, MGO, GO, MDA, or pyridoxal. Structures marked by an asterisk (*) were reported in Ref. [25] and the structure marked by a double asterisk (**) was reported in Ref. [21].

droxyimidazolidine–triazine adducts that in our case were not detected among the major adducts.[24] Under our conditions, we did not detect products for the reaction between AG and MDA, which were reported elsewhere as 5-hydroxy-2*H*-pyrazoline-1-carboxamidine (**1.8**) and its dehydrated derivative (1*H*-pyrazole-1-carboxamidine, **1.9**).[25] The product generated by AG (hydrazine group) and pyridoxal (carbonyl group) was previously reported guanyl hydrazone **1.10**.[21]

Reaction products generated by PM

The primary amino group of PM reacted with HNE to give corresponding Michael adduct **2.1** (m/z = 325.21223, Scheme 2). Under our conditions we were unable to detect the corresponding Schiff base, although previous studies suggest that the condensation of carbonyl groups with the PM primary amine should be promoted by the vicinal phenolic function, which assists the formation of the carbinolamine intermediate.[16] Phenolic and amine groups were found to be directly engaged by condensation between PM and GO, which involves two molecules for each reactant and generates piperazine-based five-ring adduct **2.2** as already described by Voziyan et al.[26] (m/z = 417.17478).

Although involving the same stoichiometry, the condensation between PM and MGO gave a totally different adduct at m/z = 385.18637, already reported by Nagaraj et al.;[27] and it is reminiscent of the methylglyoxal–lysine dimer (MOLD) and, therefore, was named MOLD-like adduct **2.3**. The different products observed upon incubation of PM with GO and MGO could be easily explained by considering that MGO is markedly more prone to yield MOLD-like adducts, as evidenced by several studies.[2] The condensation between the primary amino group of PM and MDA produced expected *N*-propenal adduct **2.4** (m/z = 223.10748), whereas no adduct was detected upon incubating PM with pyridoxal (data not shown).

Reaction products generated by HY

Similar to that observed for AG upon incubating with HNE, the hydrazine moiety of HY reacted with both the β carbon atom and the carbonyl group of HNE to yield corresponding Michael adduct **3.1** (m/z = 317.19695; Scheme 3) and phthalazinyl hydrazone **3.2** (m/z = 299.18639), respectively.

The reaction of HY with α-dicarbonyls generated very similar adducts, as GO and MGO condensed with one HY molecule to give corresponding phthalazinyl hydrazone adducts **3.3** and **3.4**, respectively (m/z = 201.07598 and 215.09236, respectively) and with two HY molecules to give corresponding dihydrazone adducts **3.5** and **3.6** (m/z = 343.14026 and 357.15638, respectively).

The hydrazine group of HY also reacted with MDA to generate *N*-propenal adduct **3.7** (m/z = 215.09249). The product gen-

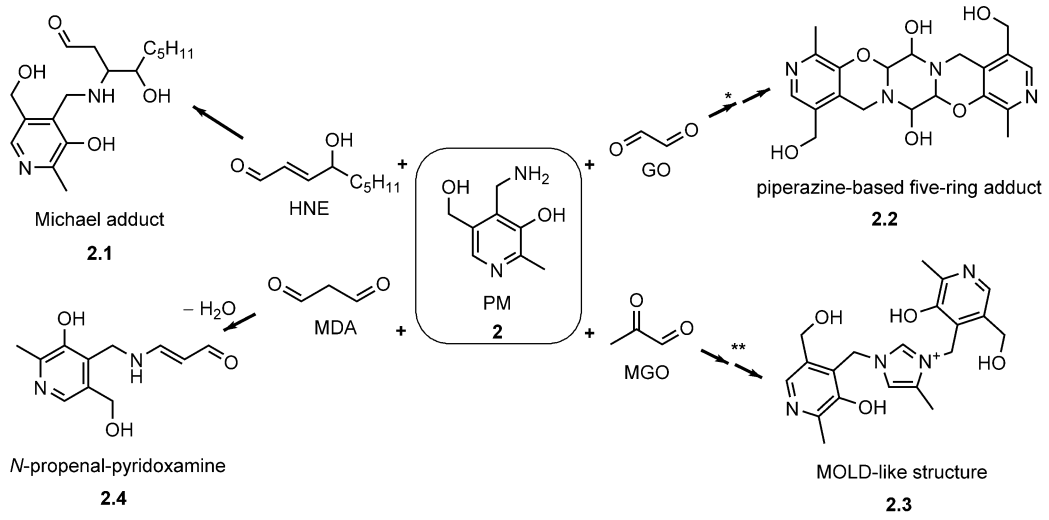

Scheme 2. Reaction products formed by pyridoxamine and HNE, MGO, GO, or MDA. The reactions marked by an asterisk (*) and a double asterisk (**) were reported in Ref. [26] and Ref. [27], respectively.

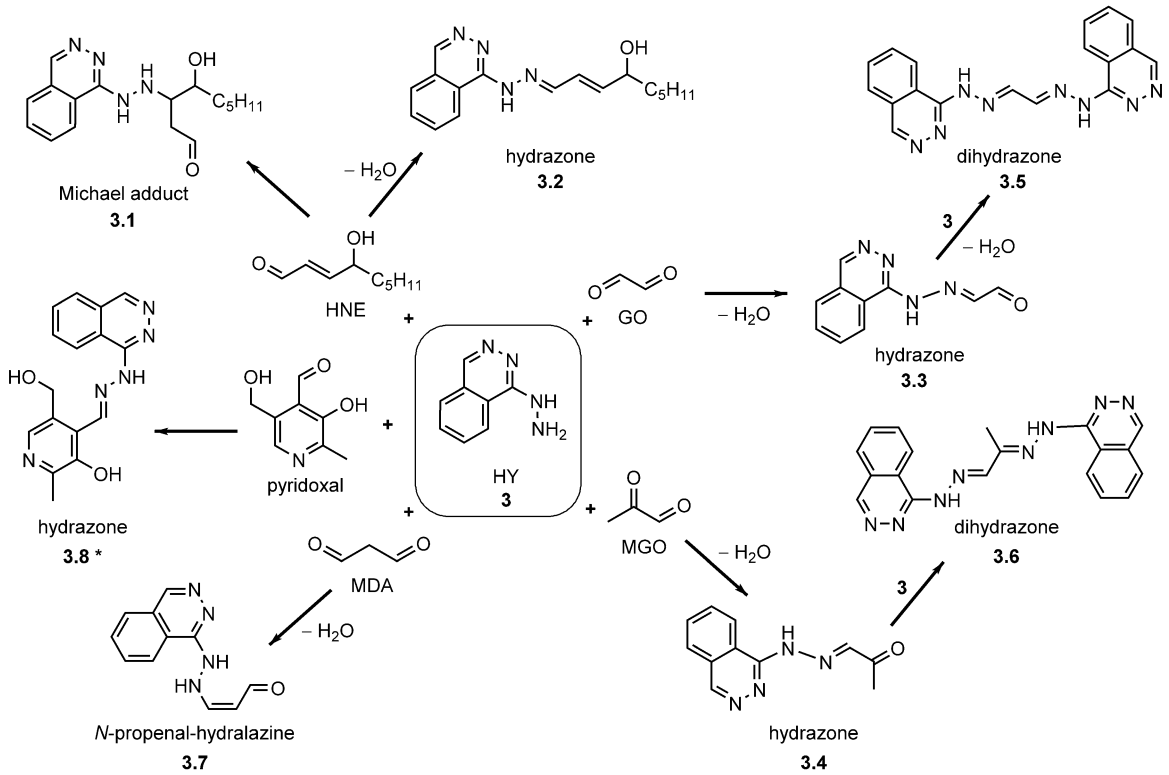

Scheme 3. Reaction products formed by hydralazine and HNE, MGO, GO, MDA, or pyridoxal. Structure marked by an asterisk (*) was reported in Ref. [26].

erated by HY (hydrazine group) and pyridoxal (carbonyl group) was previously reported phthalazinyl hydrazone **3.8**.[28]

Reaction products generated by CAR

As elucidated by previous studies,[29] the reaction between HNE and CAR followed a multistep mechanism involving the initial formation of corresponding Schiff base **4.1** (m/z = 365.21820, Scheme 4), which then underwent intramolecular Michael addition. The so-generated macrocyclic intermediate (not shown for clarity) opened and rearranged to give final Michael adduct **4.2** (m/z = 383.22854) in its hemiacetal form.

Upon incubation with both GO and MGO, the primary amino group of CAR reacted with the carbonyl groups and with the 2:2 stoichiometry described above to yield corresponding imidazole-based glyoxal–lysine dimer (GOLD)-like adduct **4.3** (m/z = 487.20212) and MOLD-like adduct **4.4** (m/z = 501.21974), respectively. Moreover, CAR condensed with GO to

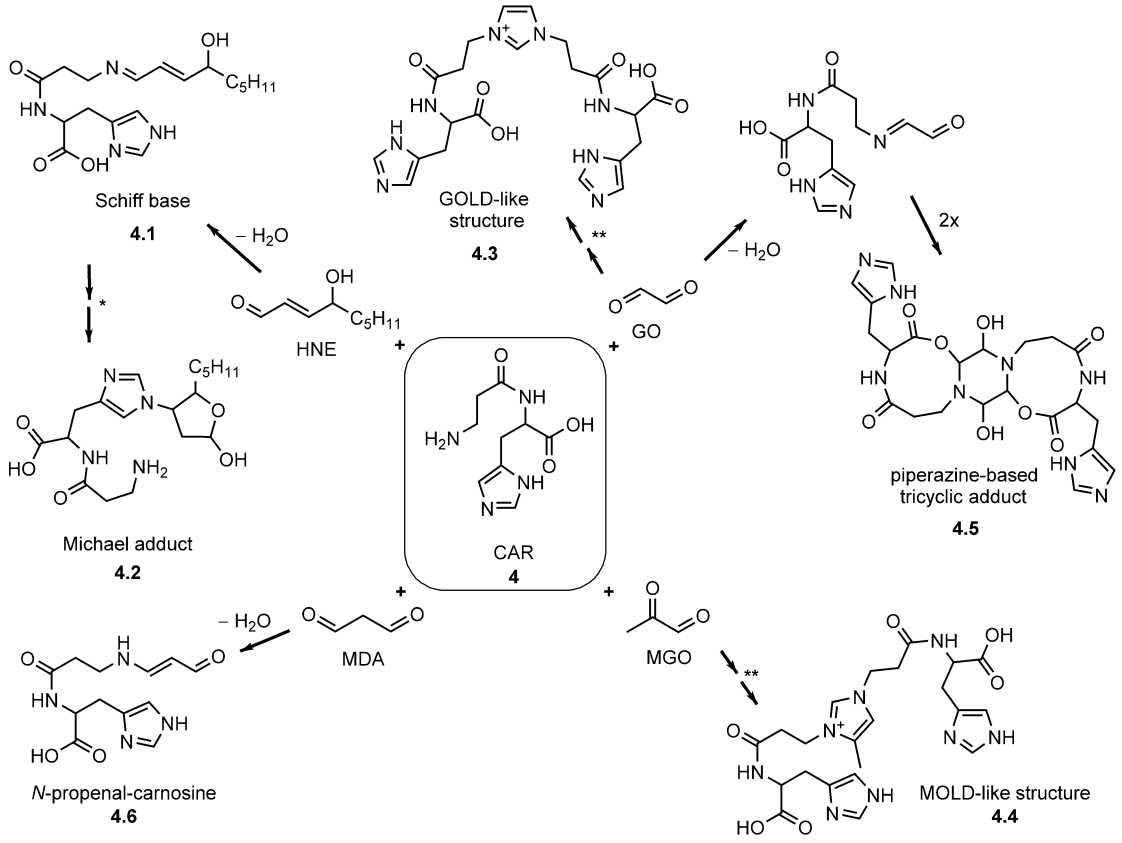

Scheme 4. Reaction products formed by carnosine and HNE, MGO, GO, and MDA. The formation of the structure marked by an asterisk (*) was characterized in Ref. [29]; the structure marked by a double asterisk (**) is based on adduct **2.3** obtained by incubating PM and MGO.

give a simple imino intermediate that then cyclized and dimerized to produce piperazine-based tricyclic adduct **4.5** (m/z = 533.20701), which is reminiscent of five-membered polycyclic adduct **2.2** obtained by incubating GO and PM. In this case, the phenolic group of PM was replaced by the carboxyl group of CAR to give a 1,3,7-oxadiazonane-6,9-dione lateral ring in place of the 1,3-oxazinane scaffold obtained with GO and PM. Notably, the condensation between suitably spaced amino acidic molecules and glyoxal to yield lactone-containing cyclic products was described by Kliegman et al. for aromatic amines.[30]

Finally, CAR reacted with MDA to generate corresponding *N*-propenal derivative **4.6** (m/z = 281.12372), whereas no adduct was detected upon incubating CAR with pyridoxal (data not shown).

Quantum-mechanical description of the selected RCS

Although the limited number of investigated compounds prevents the development of reliable quantitative structure–activity relationship (QSAR) models, the analysis of the quantum-mechanical descriptors listed in Table S2 reveals meaningful trends with the sequestering activities reported in Tables 1 (direct sequestering assay) and 2 (protein carbonylation assay). First, Table S3 shows that the reactivity towards α-dicarbonyls as measured by the protein carbonylation assay (UC_{50}) inversely correlates with the Parr's ε index for electrophilicity (r^2 = 0.86 for MGO and r^2 = 0.99 for GO). This finding confirms that the quenching of GO and MGO, although occurring through different pathways, is heavily governed by the nucleophilicity of the reactivity centers of the sequestering agents (Figure S21). By contrast, the reactivity towards α-dicarbonyls as measured by direct sequestering (R_{50}) does not correlate, which confirms that it is biased by side reactions that do not occur in the protein carbonylation experiments.

Second, the reactivity towards MDA correlates with the molecular softness (r^2 = 0.99)—a parameter that describes chemical reactivity. This result can be seen as an indirect confirmation of the similar reaction mechanisms by which the investigated quenchers react with MDA to yield the corresponding *N*-propenal adducts through Michael addition. As recently reviewed, molecular softness proves successful in predicting the reactivity/toxicity of a set of reactive carbonyl species towards a well-defined quencher.[31] Hence, it is likely that molecular softness can be suitably exploited in rationalizing the reactivity of a set of quenchers towards a given carbonyl compound (as demonstrated here). Notably, several theoretical studies have shown that molecular softness and derived local parameters are convenient descriptors to rationalize the reactivity and/or the regioselectivity of Michael additions.[32]

Third, there is no electronic descriptor in marked agreement with the reactivity towards HNE, as measured by both experi-

ments. This can be explained by considering that the quenching of HNE can involve different mechanisms (Michael addition and/or direct condensation with the carbonyl group), and thus, it is not easily accounted for by a single parameter. Hence, the sole descriptor showing moderate agreement with the reactivity towards HNE as measured in the protein carbonylation assay is the dipole moment ($r^2 = 0.44$), which probably accounts for the accessibility of the reactive groups. Again, direct HNE quenching fairly correlates with the molecular softness, a result that confirms the role of Michael addition in the reactivity toward HNE.

Finally, the reactivity towards pyridoxal is inversely correlated with Parr's ε index for electrophilicity ($r^2 = 0.87$), a result easily understandable considering that it involves a condensation reaction between the electropositive carbonyl carbon atom and a nucleophilic center of the quencher. Notably, reactivity towards α-dicarbonyls and pyridoxal appears to be governed by the same factor, and this emphasizes the difficulty in designing selective quenchers for α-dicarbonyls.

Discussion

Reaction mechanisms of sequestering agents

To our knowledge, this is the first study that compares the activities of CAR, PYR, AG, and HY towards the most widely studied RCS involved in oxidative-based diseases and belonging to three different chemical classes. All the tested RCS-sequestering agents prevented the formation of RCS-induced ubiquitin carbonylation (Figures S1–S4) by acting through a direct RCS-sequestering mechanism, as confirmed by the direct sequestering assay (Table 1) and by the identification of the reaction products (Table 3 and Figures S5–S20). The sequestering agents showed different degrees of selectivity toward the tested RCS, depending on the different reactive moieties present in both the sequestering agents and the RCS. CAR was particularly reactive with the α,β-unsaturated aldehyde 4-hydroxy-*trans*-2-nonenal, PM was reactive with malondialdehyde, AG was reactive with methylglyoxal and glyoxal, and HY efficiently quenched all RCS, also including physiological carbonyls.

The comparison of the quenching activities measured by the protein carbonylation experiments and direct sequestering assay revealed some differences that can be ascribed to kinetic factors and/or the formation of reversible/side products. Overall, these factors can be rationalized by considering that if quenchers and ubiquitin residues show roughly comparable reactivities, the two experiments produce superimposable results (as seen for HNE), whereas the two quenching activities appear to be scarcely related if the ubiquitin is markedly more reactive than the investigated quenchers (as in the case of GO/MGO with CAR).

On the basis of the reaction mechanisms and the sequestering activities, we can observe that the reactions between RCS and quenchers involving a simple 1:1 stoichiometry and multistep mechanisms make the sequestering activity most efficient. The 1,2,4-triazine and stabilized Michael adducts are examples of simple and stable products arising from multistep mechanisms, and this explains the relevant quenching capabilities of AG towards MGO/GO and CAR towards HNE. In contrast, multistep mechanisms involving a complex 2:2 stoichiometry as exemplified by MOLD/GOLD adducts for CAR with GO or the five-ring adduct for PM with GO can compete with difficulty with physiological nucleophiles, which thus explains the low reactivity of CAR and PM towards α-dicarbonyls. The involvement of such complex and kinetically disfavored reaction mechanisms can explain the lack of correlation between the two measured quenching activities, as discussed above for GO/MGO.

In general, multistep mechanisms confer a certain degree of selectivity to AG, PM, and CAR for the RCS mentioned above. Consequently, CAR was the most selective quencher owing to its peculiar mechanism of reaction with HNE, as it generates a stable product arising from a selective two-step mechanism. Conversely, reactions between RCS and quenchers involving one-step (often reversible) mechanisms are less efficient and/or less selective, as exemplified by the condensation products formed by AG/PM with HNE. A clear example of low selectivity is represented by hydralazine, which is very reactive towards all RCS through the one-step formation of hydrazone, Michael, and *N*-propenal adducts.

The in silico analysis of the selected RCS confirmed that carbonyl quenching, although a general condensation between nucleophilic and electrophilic reactants, occurs through different mechanisms that depend on the chemical nature of the trapped carbonyl species. Such a quenching mechanism is reflected by the quencher, the reactivity of which can be parameterized by specific stereoelectronic properties. As evidenced by Table S3, only the reactivity towards pyridoxal and dicarbonyls appears to be related and influenced by the same factor (i.e., nucleophilicity), whereas the reactivity towards the other monitored RCS appears to be unrelated and governed by different factors, as confirmed by the low r^2 values (always < 0.5) reported in Table S1. This may explain why AG and HY, which are very effective quenchers for dicarbonyls, also deplete the physiological carbonyls, whereas CAR and PM, which are less effective towards dicarbonyls, show the desired selectivity. The obtained results emphasize that a specific quenching might be pursued by modulating well-defined electronic properties that can thus be seen as guiding factors in the rational design of optimized carbonyl quenchers.

It should be considered that the covalent adducts described above, including the Michael adducts, were found to be stable under our in vitro conditions, but their formation can be reversed under physiological conditions owing to the presence of high concentrations of strong nucleophilic agents. In such a context, it is possible that physiological enzymes can stabilize the reversible reaction products, including the Michael adducts, which would thus enhance the overall quenching activity. Very recently, Baba et al. found that aldose reductase plays a role in the metabolism and detoxification of carnosine–acrolein conjugates.[33] In particular, they reported that conjugates of carnosine with aldehydes such as acrolein are produced during normal metabolism, excreted in the urine of mice and adult human nonsmokers as carnosine–propanols, and that

the reduction of carnosine–propanals is catalyzed by the enzyme aldose reductase. Reduction of aldehyde moieties clearly stabilizes the adducts and catalyzes their formation. More investigation into the role of enzymes in the detoxification mechanisms of RCS-sequestering agents is needed.

Conclusions

On the basis of the results mentioned above, we can conclude that the reactive carbonyl species (RCS) trapping activity of most of the sequestering agents reported in the literature so far depends on the target RCS. Hence, the choice of the sequestering agent for the treatment of a disease should be driven by the main RCS produced in that particular disease and that a rational combination of RCS-sequestering agents should be considered if different classes of RCS are involved.

Our findings also highlight a rational approach for the design of novel sequestering agents. Selectivity represents the first important prerequisite of a suitable sequestering agent, which is obtained by avoiding reactive moieties able to form a covalent adduct with the target RCS through a single reaction step, as in the case of hydralazine. A multistep mechanism should be considered and based on at least two reaction moieties, the selection of which should be based on the functional groups present in the target aldehyde. A typical example of selectivity is given by carnosine, which acts through two reactive moieties (the N atom of the imidazole ring and the amino group of the β-alanine residue) targeting the two reactive sites of α,β-unsaturated aldehydes, the aldehyde function and the electrophilic C3 atom. Rational design should also take into account any enzymatic reaction that can occur in vivo and that can catalyze the sequestering activity of the agent, as in the case of aldose reductase, which stabilizes in vivo the Michael adduct formed by the reaction of carnosine with α,β-unsaturated aldehydes by reducing the carbonyl moiety.

Finally, the present paper highlights the importance of analytical methods to assess the ability of compounds to inhibit RCS-mediated carbonylation. The measurement of RCS consumption (a widely used test) is useful, as it allows understanding of the intrinsic reactivity of a tested compound as a sequestering agent, but it is limited, because it can only be applied to UV/Vis-detectable RCS targets and because in some cases it is not a suitable model to predict the effect on protein carbonylation. We conclude that to have a complete picture, the direct sequestering test needs to be integrated with a model able to assess the inhibitory effect on protein carbonylation, such as the ubiquitin model reported herein.

Experimental Section

General

Ultrapure water was prepared with a Milli-Q H_2O purification system (Millipore, Bedford, USA). Sodium dihydrophosphate ($NaH_2PO_4{\cdot}H_2O$), disodium phosphate ($Na_2HPO_4{\cdot}2H_2O$), ammonium bicarbonate (NH_4HCO_3), formic acid (HCOOH), sodium borohydride ($NaBH_4$), LC–MS-grade H_2O/0.1% formic acid, LC–MS-grade methanol, LC–MS-grade acetonitrile, LC–MS-grade acetonitrile with 0.1% formic acid, lyophilized ubiquitin from bovine erythrocytes (U6253), methylglyoxal (67028), glyoxal (50649), malondialdehyde tetrabutylammonium salt (63287), pyridoxamine dihydrochloride (P9380), hydralazine hydrochloride (H1753), aminoguanidine hydrochloride (396494), and 2,5-hexanedione (165131) were purchased from Sigma–Aldrich (Milan, Italy). L-Carnosine was obtained from Flamma S.p.A. (Chignolo d'Isola, Italy). 4-Hydroxy-2-nonenal dimethyl acetal was synthesized according to the literature[34] and was stored at −20 °C. For each experiment, fresh 4-hydroxy-2-nonenal was prepared as previously described.[17]

Analytical methods

Sequestering activity: HPLC analysis

The reactivity of each sequestering agent toward HNE was directly evaluated by measuring its consumption by HPLC–UV analysis (Surveyor HPLC, Thermo Finnigan Italia S.p.A., Milan, Italy equipped with an UV6000 LP photodiode array detector/PDA). The selectivity was evaluated by a similar approach, for which pyridoxal was used instead of HNE to represent an endogenous aldehyde. Samples were prepared by incubating each sequestering agent with HNE or pyridoxal (100 μM in 10 mM phosphate buffer, pH 7.4) at different molar ratios (from 1:10 to 10:1) for 24 h at 37 °C. Separation was obtained by reverse-phase chromatography (Synergi Fusion column, 150 mm × 2 mm, 4 μm) protected by a RP SecurityGuard (both from Phenomenex, Inc., Castel Maggiore, Italy) at 37 °C by using Na_2HPO_4 10 mM pH 7.4/CH_3CN, 40:60 *v/v* as the mobile phase at a flow rate of 0.25 mL min^{-1}. The PDA detector was set at $\lambda = 224$ nm, which corresponds to the maximum absorbance wavelength of HNE.

MGO quenching activity was evaluated as described above, but by using 1 mM MGO and a Hypercarb column (100 mm × 2.1 mm, 3 μm, Thermo scientific, Pobbiano, Italy). MGO was eluted by using a linear gradient starting from 95% H_2O/5% methanol to 50% H_2O/50% methanol over 5 min at flow rate of 0.3 mL min^{-1}. The PDA detector was set at $\lambda = 285$ nm, which corresponds to the maximum absorbance wavelength of MGO.

The quenching activities towards HNE, MGO, and pyridoxal is reported as the percentage of consumption (Q%) determined by mixing the sequestering agent and the RCS at different molar ratios (e.g., $Q\%_{1:1}$ refers to ratio 1:1) and by calculating the molar ratio (R_{50}) at which each sequestering agent consumed 50% of the tested RCS.

Inhibition of carbonylation: in vitro incubation and MS-based analysis

Sample preparation: 10 μM ubiquitin was incubated at 37 °C in 10 mM phosphate buffer pH 7.4 in the presence of 500 μM HNE, 500 μM GO, 100 μM MGO, or 5 mM MDA together with one of the following sequestering agents: hydralazine, aminoguanidine, pyridoxamine, or L-carnosine, at different concentrations. The RCS concentrations were selected to yield approximately 50% of RCS-carbonylated ubiquitin;[18] RCS molarity corresponds to an excess (over ubiquitin molarity) equal to 50× for HNE and GO, 10× for MGO, and 500× for MDA. 10 μM ubiquitin was incubated without RCS as a blank sample. Control samples were prepared by incubating 10 μM ubiquitin with 500 μM HNE, 500 μM GO, 100 μM MGO, or 5 mM MDA, without any quencher. The reactions were stopped after 24 h by centrifugation by using Amicon YM3 filter units (Millipore, Milan, Italy), as already described.[17] After buffer exchange,

the sample was, if necessary, brought up to the initial volume (70 μL) with water. Each assay was repeated three times to produce three independent replicates.

Intact protein analysis by microflow automated loop injection ESI-MS: Intact ubiquitin (either in its unmodified or RCS-modified forms) was analyzed by HRMS as already described.[17] Briefly, ubiquitin solution (40 μL) recovered from filter units was mixed with denaturing solution (40 μL) ($H_2O/CH_3CN/HCOOH$; 40/60/0.2 *v/v/v*). Aliquots of the samples (5 μL) were injected into an LTQ-Orbitrap XL mass spectrometer by using an ESI source (Thermo Scientific, Milan, Italy). Samples were automatically injected by an Ultimate 3000 RSLCnano system at a constant flow rate of 10 μL min^{-1} of $H_2O/CH_3CN/HCOOH$; 70/30/0.1 *v/v/v*. Sample injection and spectra acquisition were fully automated and were controlled by Xcalibur software (version 2.0.7, Thermo Scientific) and Chromeleon Xpress software (Dionex, version 6.80). Source parameters: spray voltage 1.8 kV, capillary temperature 220 °C, capillary voltage 35 V, tube lens offset 120 V. A list of 20 background ions was used as lock mass values for real-time mass calibration.[35] Mass spectra were acquired by the Orbitrap analyzer in the positive-ion mode by using the profile mode, scan range m/z = 110–2000, AGC target 5×10^5, maximum inject time 500 ms, resolving power 100 000 (full width at half maximum (FWHM) at m/z = 400). Each sample was acquired three times to obtain three technical replicates.

Quantification of the extent of carbonylation: A dedicated Xcalibur processing method was set to quantify the area under the +11 multicharged peaks,[17] localized in the ranges m/z = 779.00–783.50 for unmodified ubiquitin, m/z = 793.00–797.50 for HNE-modified ubiquitin, m/z = (784.25–785.75) + (789.50–791.00) + (794.75–796.25) for GO-modified ubiquitin, m/z = 784.00–787.00 for MGO-modified ubiquitin, and m/z = (784.00–785.50) + (788.10–789.60) for MDA-modified ubiquitin. Peak areas were automatically detected and quantified postacquisition by using an Xcalibur Quan Browser (Thermo Scientific). The percentage of modified ubiquitin contained in each sample was computed according to Equation (1):

$$\%\ \text{Modified ubiquitin} = \left[\frac{\text{AUC-modified ubiquitin}}{(\text{AUC-unmodified ubiquitin} + \text{AUC-modified ubiquitin})}\right] \times 100 \quad (1)$$

The percentage of modified ubiquitin obtained upon co-incubation with RCS and carbonyl quenchers was normalized against the percentage of modified ubiquitin obtained in the control samples (ubiquitin incubated with RCS without any quencher). The noise present in the blank sample (ubiquitin incubated without RCS) was subtracted.

The percentages of modified ubiquitin were plotted against the log concentration of quencher (expressed as quencher/RCS molar ratio). The concentration of carbonyl quenchers able to inhibit the formation of adducts on ubiquitin by 50% was obtained by interpolating the concentration–response curve (GraphPad Software Inc., version 6.04): such concentration was termed UC_{50} and is expressed as the quencher/RCS molar ratio.

HRMS and computational analyses for elucidation of reaction products

Sample preparation: Each RCS was incubated at 37 °C with each carbonyl quencher at different molar ratios, which were previously optimized to enhance the formation of detectable amounts of products. HNE was incubated with all quenchers in a 1:1 ratio. MGO and GO were incubated at a 1:1 ratio with AG, HY, and PM, a 1:5 ratio with HY, and 10:1 and 5:1 ratios with CAR. MDA was incubated with CAR, HY, and PM at a 1:1 ratio, a 1:5 ratio with HY, and 10:1 and 5:1 ratios with AG. Control samples contained the single RCS or quencher at 800 μM concentration in 1 mM phosphate buffer, pH 7.4.

MS-based analysis of RCS/quencher reaction products: After 24 h incubation, all samples were diluted approximately 10-fold in water and were directly infused into the LTQ-Orbitrap XL by using a microliter syringe (Hamilton, Bonaduz, Switzerland) at a flow rate of 10 μL min^{-1}. The ESI source (Thermo Scientific, Milan, Italy) was set as follows: spray voltage 3.5 kV, sheath gas 5, capillary temperature 275 °C, capillary voltage 35 V, tube lens offset 120 V. The lock mass option was enabled. Spectra were acquired by using the Tune Plus software (version 2.4 SP1, Thermo). Full mass spectra were acquired by the Orbitrap (FT) analyzer in the positive-ion mode by using the following settings: profile mode, scan range m/z = 60–600, AGC target 5×10^5, maximum inject time 500 ms, resolving power 100 000 (FWHM at m/z = 400). Full mass spectra were acquired for 30 s to average signals. If the Orbitrap analyzer did not detect the signal, full mass spectra were acquired by using the LTQ-XL analyzer in the range m/z = 50–600, with AGC target 5×10^4, maximum inject time 100 ms. Most abundant peaks were fragmented to obtain MS/MS spectra by using a selection window of 2.5 m/z. We used both CID and HCD fragmentation (with AGC target = 1×10^4 or 2×10^5, respectively); the collision energy was experimentally adjusted for each precursor to increase the signal of the fragment ions (generally CE = 35–55 V). Most fragmentation products were acquired by using the Orbitrap analyzer at a resolving power 100 000 (FWHM at m/z = 400). In a few cases, if the Orbitrap analyzer did not detect the signal, we acquired MS/MS spectra with the LTQ-XL analyzer. Full mass spectra were acquired for 30 s to average signals.

In silico generation of reaction product fragments: We assigned a chemical structure to each product obtained from the RCS/quencher reaction on the basis of the data obtained from the literature and on the highly accurate mass values observed by HRMS. Elemental composition was obtained by the Xcalibur/Qual Browser software by using a 8 ppm tolerance. The structure was drawn by using ChemSketch software (version 12.01, Advanced Chemistry Development, Canada) and imported into the Highchem—MassFrontier software (version 5.1, Thermo Scientific) that generated theoretical fragments according to both general chemistry rules and HighChem fragmentation library. We used the default setting, with the following exceptions: radical species were excluded from the analyses, maximum four fragmentation steps were allowed, and the minimum mass value was 50 Da. The mass values of the theoretical fragments were compared with the experimental values, with a tolerance equal to 8 ppm for spectra acquired by the Orbitrap analyzer and 0.3 Da for spectra acquired by the LTQ-XL analyzer.

Molecular modeling of the investigated RCS: Owing to their markedly different flexibility, the stereoelectronic properties of the carbonyl quenchers were investigated by exploiting different computational strategies. Indeed, the more rigid sequestering agents AG, HY, and PYR were analyzed by considering only the lowest-energy conformation as derived by quenched MonteCarlo simulations (generating 1000 minimized geometries by randomly rotating the rotors) followed by PM7 semiempirical optimization, whereas for the more-flexible CAR, 15 nonredundant favored conformations were generated by the MonteCarlo search and optimized by semiempirical calculations. All so-generated conformations were finally minimized at their ground state and in the gas phase by density

functional theory (DFT) by using the Becke three-parameter hybrid function with LYP correlation (DFT/B3LYP) and with the 6-31G basis set as implemented by the GAMESS software. These calculations provided dipole moments, HOMO and LUMO energies, and the so-derived molecular softness, chemical potential and Parr's ω and ε electrophilicity indices (reported in Table S2).

Acknowledgements

M.C. received a postdoctoral fellowship from the Dote Ricerca (FSE, Regione Lombardia, Italy) enabling her to carry out the work described herein.

Keywords: carbonyl quenching · liquid chromatography · mass spectrometry · molecular modeling · reactive carbonyl species

[1] G. Aldini, I. Dalle-Donne, R. M. Facino, A. Milzani, M. Carini, *Med. Res. Rev.* **2007**, *27*, 817 – 868.
[2] G. Vistoli, D. De Maddis, A. Cipak, N. Zarkovic, M. Carini, G. Aldini, *Free Radical Biol. Med.* **2013**, *47*, 3 – 27.
[3] I. Dalle-Donne, R. Rossi, D. Giustarini, A. Milzani, R. Colombo, *Clin. Chim. Acta* **2003**, *329*, 23 – 38.
[4] a) I. Dalle-Donne, G. Aldini, M. Carini, R. Colombo, R. Rossi, A. Milzani, *J. Cell. Mol. Med.* **2006**, *10*, 389 – 406; b) A. Prasad, P. Bekker, S. Tsimikas, *Cardiol. Rev.* **2012**, *20*, 177 – 183; c) J. R. Requena, M. X. Fu, M. U. Ahmed, A. J. Jenkins, T. J. Lyons, S. R. Thorpe, *Nephrol. Dial. Transplant.* **1996**, *11*, 48 – 53.
[5] a) R. Vatsyayan, H. Kothari, U. R. Pendurthi, L. V. Rao, *Arterioscler. Thromb. Vasc. Biol.* **2013**, *33*, 1601 – 1611; b) S. Del Turco, G. Basta, *Biofactors* **2012**, *38*, 266 – 274.
[6] a) D. Suzuki, T. Miyata, N. Saotome, K. Horie, R. Inagi, Y. Yasuda, K. Uchida, Y. Izuhara, M. Yagame, H. Sakai, K. Kurokawa, *J. Am. Soc. Nephrol.* **1999**, *10*, 822 – 832; b) A. Goldin, J. A. Beckman, A. M. Schmidt, M. A. Creager, *Circulation* **2006**, *114*, 597 – 605; c) P. A. Grimsrud, M. J. Picklo, T. J. Griffin, D. A. Bernlohr, *Mol. Cell. Proteomics* **2007**, *6*, 624 – 637.
[7] R. Sultana, M. Perluigi, D. Allan Butterfield, *Free Radical Biol. Med.* **2013**, *62*, 157 – 169; J. T. Keeney, A. M. Swomley, S. Förster, J. L. Harris, R. Sultana, D. A. Butterfield, *Proteomics Clin. Appl.* **2013**, *7*, 109 – 122.
[8] a) G. Aldini, M. Orioli, G. Rossoni, F. Savi, P. Braidotti, G. Vistoli, K. J. Yeum, G. Negrisoli, M. Carini, *J. Cell. Mol. Med.* **2011**, *15*, 1339 – 1354; b) M. Takeuchi, J. Takino, S. Yamagishi, *Curr. Drug Targets* **2010**, *11*, 1468 – 1482; c) M. Orioli, G. Vistoli, L. Regazzoni, A. Pedretti, A. Lapolla, G. Rossoni, R. Canevotti, L. Gamberoni, M. Previtali, M. Carini, G. Aldini, *ChemMedChem* **2011**, *6*, 1269 – 1282.
[9] G. Aldini, G. Vistoli, M. Stefek, N. Chondrogianni, T. Grune, J. Sereikaite, I. Sadowska-Bartosz, G. Bartosz, *Free Radical Res.* **2013**, *47*, 93 – 137.
[10] G. Aldini, M. Carini, K. J. Yeum, G. Vistoli, *Free Radic. Biol. Med.* **2014**, *69*, 145 – 156.
[11] a) H. T. Nagasawa, J. A. Elberling, E. G. DeMaster, *J. Med. Chem.* **1980**, *23*, 140 – 143; b) G. T. Wondrak, D. Cervantes-Laurean, M. J. Roberts, J. G. Qasem, M. Kim, E. L. Jacobson, M. K. Jacobson, *Biochem. Pharmacol.* **2002**, *63*, 361 – 373.
[12] D. Ruggiero-Lopez, M. Lecomte, G. Moinet, G. Patereau, M. Lagarde, N. Wiernsperger, *Biochem Pharmacol* **1999**, *58*, 1765 – 1773.
[13] P. C. Burcham, F. R. Fontaine, L. M. Kaminskas, D. R. Petersen, S. M. Pyke, *Mol. Pharmacol.* **2004**, *65*, 655 – 664.
[14] a) G. Vistoli, M. Carini, G. Aldini, *Amino Acids* **2012**, *43*, 111 – 126; b) S. V. Chetyrkin, W. Zhang, B. G. Hudson, A. S. Serianni, P. A. Voziyan, *Biochemistry* **2008**, *47*, 997 – 1006; c) R. Mehta, L. Wong, P. J. O'Brien, *Chem.-Biol. Interact.* **2009**, *178*, 317 – 323; d) C. H. Shao, G. J. Rozanski, R. Nagai, F. E. Stockdale, K. P. Patel, M. Wang, J. Singh, W. G. Mayhan, K. R. Bidasee, *Biochem. Pharmacol.* **2010**, *80*, 205 – 217.
[15] a) M. Orioli, G. Aldini, M. C. Benfatto, R. M. Facino, M. Carini, *Anal. Chem.* **2007**, *79*, 9174 – 9184; b) G. Colombo, G. Aldini, M. Orioli, D. Giustarini, R. Gornati, R. Rossi, R. Colombo, M. Carini, A. Milzani, I. Dalle-Donne, *Antioxid. Redox Signaling* **2010**, *12*, 349 – 364.
[16] C. Caldés, B. Vilanova, M. Adrover, F. Muñoz, J. Donoso, *Chem. Biodiversity* **2011**, *8*, 1318 – 1332.
[17] M. Colzani, A. Criscuolo, D. De Maddis, D. Garzon, K. J. Yeum, G. Vistoli, M. Carini, G. Aldini, *J. Pharm. Biomed. Anal.* **2014**, *91C*, 108 – 118.
[18] M. Colzani, A. Criscuolo, G. Casali, M. Carini, G. Aldini, *Free Radical Res.* **2016**, *50*, 328 – 336.
[19] R. J. Schaur, *Mol Aspects Med* **2003**, *24*, 149 – 159.
[20] P. C. Rumsby, D. M. Shepherd, *Br. J. Pharmacol.* **1979**, *67*, 453P – 454P.
[21] T. Taguchi, M. Sugiura, Y. Hamada, I. Miwa, *Biochem. Pharmacol.* **1998**, *55*, 1667 – 1671.
[22] M. D. Neely, L. Zimmerman, M. J. Picklo, J. J. Ou, C. R. Morales, K. S. Montine, V. Amaranth, T. J. Montine, *Free Radical Biol. Med.* **2000**, *29*, 1028 – 1036.
[23] P. J. Thornalley, A. Yurek-George, O. K. Argirov, *Biochem. Pharmacol.* **2000**, *60*, 55 – 65.
[24] M. A. Saraiva, C. M. Borges, M. H. Florêncio, *Eur. J. Mass Spectrom.* **2012**, *18*, 385 – 397.
[25] Y. Al-Abed, R. Bucala, *Chem. Res. Toxicol.* **1997**, *10*, 875 – 879.
[26] P. A. Voziyan, T. O. Metz, J. W. Baynes, B. G. Hudson, *J. Biol. Chem.* **2002**, *277*, 3397 – 3403.
[27] R. H. Nagaraj, P. Sarkar, A. Mally, K. M. Biemel, M. O. Lederer, P. S. Padayatti, *Arch. Biochem. Biophys.* **2002**, *402*, 110 – 119.
[28] N. H. Raskin, R. A. Fishman, *N. Engl. J. Med.* **1965**, *273*, 1182 – 1185.
[29] G. Aldini, M. Carini, G. Beretta, S. Bradamante, R. M. Facino, *Biochem. Biophys. Res. Commun.* **2002**, *298*, 699 – 706.
[30] J. M. Kliegman, R. K. Barnes, *J. Org. Chem.* **1970**, *35*, 3140 – 3143.
[31] R. M. LoPachin, T. Gavin, *Chem. Res. Toxicol.* **2014**, *27*, 1081 – 1091.
[32] G. Madjarova, A. Tadjer, T. P. Cholakova, A. A. Dobrev, T. Mineva, *J. Phys. Chem. A* **2005**, *109*, 387 – 393.
[33] S. P. Baba, J. D. Hoetker, M. Merchant, J. B. Klein, J. Cai, O. A. Barski, D. J. Conklin, A. Bhatnagar, *J. Biol. Chem.* **2013**, *288*, 28163 – 28179.
[34] M. Rees, F. Vankuijk, A. Siakotos, B. Mundy, *Synth. Commun.* **1995**, *25*, 3225 – 3236.
[35] B. O. Keller, J. Sui, A. B. Young, R. M. Whittal, *Anal. Chim. Acta* **2008**, *627*, 71 – 81.

Received: November 24, 2015
Revised: January 19, 2016
Published online on ■■ ▮▮, 0000

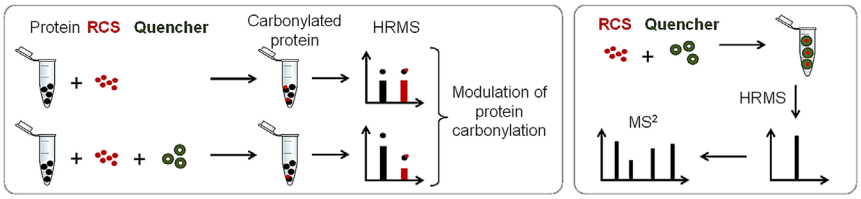

Carbonyl quenchers: A protein carbonylation assay is used to quantify the extent of modification of a model protein upon its in vitro incubation with fixed concentrations of different reactive carbonyl species (RCS) and increasing concentrations of sequestering agents. The assay shows preferential reactivity of some sequestering agents versus given RCS. The reaction products obtained from the RCS and the sequestering agents are identified by HRMS.

M. Colzani, D. De Maddis, G. Casali, M. Carini, G. Vistoli, G. Aldini*

■■ – ■■

Reactivity, Selectivity, and Reaction Mechanisms of Aminoguanidine, Hydralazine, Pyridoxamine, and Carnosine as Sequestering Agents of Reactive Carbonyl Species: A Comparative Study